J. Fluid Mech. (1989), *vol.* 200, *pp.* 95–120
Printed in Great Britain

The dynamics of the near field of strong jets in crossflows

By SERGIO L. V. COELHO[1]† AND J. C. R. HUNT[2]

[1] Department of Engineering, University of Cambridge, Trumpington Street, Cambridge CB2 1PZ, UK

[2] Department of Applied Mathematics and Theoretical Physics, University of Cambridge, Silver Street, Cambridge CB3 9EW, UK

(Received 27 April 1987 and in revised form 1 June 1988)

An inviscid three-dimensional vortex-sheet model for the near field of a strong jet issuing from a pipe into a crossflow is derived. The solution for this model shows that the essential mechanisms governing this idealized flow are the distortion of the main transverse vorticity by the generation of additional axial and transverse vorticity within the pipe owing to the pressure gradients induced by the external flow, and the convection of both components of vorticity from the upwind side of the jet to its downwind side.

The deformation of the cross-section of the jet which is predicted by this model is compared with the deformation predicted by the commonly used time-dependent two-dimensional vortex-sheet model. Differences arise because the latter model does not take into account the effects of the transport of the transverse component of vorticity. The complete three-dimensional vortex-sheet model leads to a symmetrical deformation of the jet cross-section and no overall deflection of the jet in the direction of the stream.

To account for viscous effects, the initial region of a strong jet issuing into a uniform crossflow is modelled as an entraining three-dimensional vortex sheet, which acts like a sheet of vortices and sinks, redistributing the vorticity in the bounding shear layer and inducing non-symmetrical deformations of the cross-section of the jet. This leads to a deflection of the jet in the direction of the stream, and the loci of the centroids of the cross-sections of the jet describe a quadratic curve.

Deformations predicted by each of the three models are compared with measurements obtained from photographs of the cross-sections of a jet of air emerging into a uniform crossflow in a wind tunnel. Mean velocity measurements around the jet made with a hot-wire anemometer agree with the theory; they clearly invalidate models of jets based on 'pressure drag'.

1. Introduction

The issuing of jets into deflecting streams has been the subject of numerous studies because of its wide variety of applications in engineering. Chimney plumes for the dispersion of pollutants in the atmosphere, the cooling of turbine blades, lifting jets for V/STOL aircrafts and jets of oil and gas entering the flow in oil wells are just a few important examples.

Observations of the initial region of turbulent jets discharging from circular pipes

† Present address: Programma de Mecanica, COPPE/UFRJ, Cidade Universitairia, CP 68503-CEP 21945, Rio de Janeiro, Brazil.

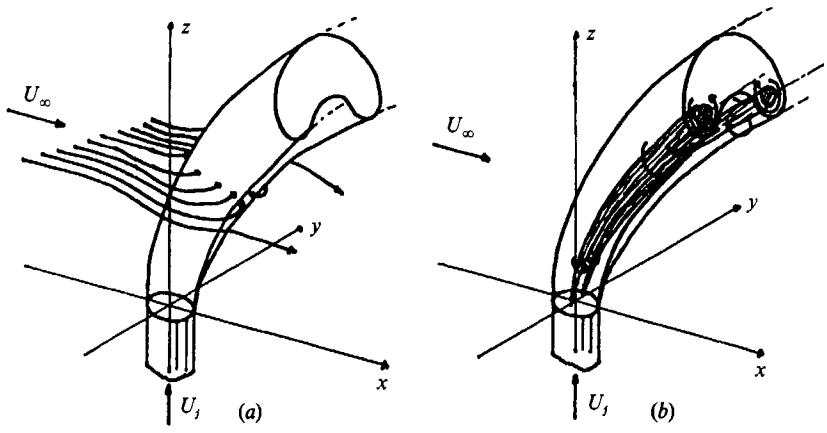

FIGURE 1. Models for a jet in a crossflow: (*a*) entraining surface; (*b*) vortex pair.

or orifices show that, first, the cross-sectional area increases as the jet entrains fluid from the external stream and, secondly, the shape of the cross-section changes into a horseshoe. The tips of these horseshoes evolve then into a pair of contrarotating trailing vortices (that approach asymptotically the direction of the external stream in the far field of the flow) with vorticity parallel to the trajectory of the jet. At the same time, the jet begins to bend over in the direction of the crossflow.

Clearly, the dominant features in this initial region are the entrainment by the jet shear layer, and the concentration of vorticity on the downwind side of the jet. Nevertheless, few attempts have been made to describe the mechanisms leading to such behaviour, and questions of how and why turbulent jets bend over when they enter cross-streams have not yet been satisfactorily answered.

Despite the many practical fluid-mechanics problems where solutions depend on understanding the behaviour of jets, quite different answers to these questions have been given in different fields of application, based on different explanations of the mechanics of the flow. This fact reduces one's confidence in many current models based on these different explanations. It is important that there is a basic understanding of the mechanisms that govern the motion of simple turbulent jets issuing normally to uniform crossflows before one can have confidence in the use of current models for jet flows in more complex situations.

Models for the jet based on completely different approaches have been presented in the literature. In environmental fluid mechanics the jet flow is usually modelled by an integral approach, where an entraining control surface is assumed for the jet; aerodynamicists have also used integral approaches, modelling the flow as a pair of contrarotating vortex filments or tubes in a cross-stream (e.g. Durando 1971; Broadwell & Breidenthal 1984; Karagozian & Greber 1984). Schematic representations of models are shown in figure 1. Satisfactory agreement with experimental data for the trajectory of the jet has been reported with both approaches. In these integrals models, however, no attempt to match the internal and the external flows has been made and only the trajectory and the overall size of the jet have been calculated. Suitable entrainment functions and coefficients and/or suitable drag coefficients provide satisfactory calculations for the trajectory of the jet, regardless of the assumptions made with respect to the mechanisms responsible for the deflection of the jet. In some of these models, the mechanisms is assumed to be pressure drag (e.g. Endo 1974; Sucec & Bowley 1976; Makihata & Miyai 1979);

addition of momentum by means of entrainment is the assumed mechanism in some other models (e.g. Platten & Keffer 1968; Hoult & Weil 1972); both mechanisms are considered by Schatzman (1978) and Adler & Baron (1979).

The results obtained with the above-mentioned models show that similar trajectories for the jet seem to be predicted even when the dominant mechanisms are assumed to be quite different. The lack of any detailed comparison of the flow predicted by these models with experimental data mean that no firm conclusion can be drawn as to which are the key mechanisms for the deflection, distortion and formation of the trailing vortex pair of the jet.

Previous theoretical investigations on the formation of the vortex pair have been based on the time-evolving two-dimensional vortex-sheet model introduced by Chang-Lu (1942). In these models, the flow in and outside the jet is assumed to be potential flow and the boundary between them to be a vortex sheet. The additional hypothesis is made that the form of the three-dimensional vortex sheet can be approximated by a two-dimensional one that evolves in time, and a uniform velocity at the nozzle is assumed as the initial condition.

Discretizing this vortex sheet into a number of vortex filaments that are essentially aligned with the trajectory of the jet, Margason (1969) evaluated the cross-sectional distortion via a numerical computation of the movement of these vortex filaments. The transport of vorticity predicted by these models causes vorticity to concentrate on the downwind side of the vortex sheet, leading to a roll-up process that reflects some of the qualitative features present in real jets. However, according to these models, the vortex pair is formed by the concentration of the streamwise component of vorticity only; the transverse component has no effect in this process. This leads to a total circulation which is independent of the velocity ratio; this is a clear disagreement with the experimental data from Fearn & Weston (1974).

The probable reasons for the disagreement between these models and detailed measurements are that turbulent entrainment is ignored, and that a two-dimensional approximation is assumed for a fully three-dimensional vortex-sheet problem. It is worth mentioning that the validity of this two-dimensional approximation for the fully three-dimensional problem appears to be based on intuitive arguments only and no formal analysis to support it has been presented in the literature.

In this paper, a new analysis of the dynamics of the near field of a strong jet issuing into a uniform crossflow is presented. The flow in this region allows for a rather rigorous analysis of the mechanisms involved in the deflection and distortion of the jet and also in the formation of the pair of trailing vortices. In the initial region, the deflection and distortion of the jet are still small, entrainment is still limited to a thin mixing layer at its boundary, and the vortex pair is still only beginning to be formed.

The commonly used unsteady two-dimensional inviscid model (Chang-Lu's model) for this region is compared with the fully three-dimensional model for the inviscid flow it supposedly describes. It is shown that these two models do not give the same description of this theoretical flow, and that the correct three-dimensional solution for this inviscid approach of jets in crossflows does not describe the real flow. A satisfactory description is only obtained when this three-dimensional inviscid model is modified to incorporate the effects of turbulent entrainment.

First, we shall develop an analytic solution which describes the behaviour of Chang-Lu's model for small times. Chang-Lu's model is based on the same parameterization of the trajectory of the jet with respect to time as is used in the vortex-pair approach for the far field of the flow. It models the jet as two regions of

irrotational flow separated by a vortex sheet that evolves in time. With this approach, the interaction of the jet with the external flow is equivalent to that of a cylinder of fluid about which an external flow is impulsively started. This equivalence is apparently based on intuitive arguments only, and no formal analysis supporting it has been presented in the literature.

Then, a fully three-dimensional inviscid solution for the vortex-sheet model for the initial region of the jet is derived, and it is shown how it differs from the solution given by Chang-Lu's two-dimensional time-dependent approximation. The three-dimensional model includes the development of the flow out of the pipe into the jet, and shows how additional axial and transverse components of vorticity are generated at the pipe wall near its exit. It is found that there can be *no deflection* of the jet if it is modelled by the vortex-sheet approximation (this negative result is in agreement with the recent inviscid analysis of Needham, Riley & Smith 1988). Chang-Lu's model does predict a deflection of the jet but it is shown here that it is an incorrect approximation for the fully three-dimensional vortex-sheet model in the near field of the flow.

Finally, this three-dimensional model is used as the basis for a model incorporating the effects of turbulent entrainment. This indeed leads to the deflection of the jet because of the addition of the momentum brought in by the entrained fluid. This is the mechanism of deflection assumed by Platten & Keffer (1968) and Hoult & Weil (1972) in their integral models.

Photographs and measurements of the structure of a circular turbulent jet in a crossflow near the jet exit were obtained in a wind tunnel and are compared with the jet distortions described by each of the present models: two-dimensional time-evolving vortex sheet, three-dimensional vortex sheet, and the 'entraining vortex-sheet' model (where turbulent entrainment is considered). The experimental procedure for obtaining the photographs is outlined in §7.

2. The two-dimensional vortex-sheet model

Chang-Lu's inviscid two-dimensional time-dependent approximation produces a mathematical model equivalent to that for a two-dimensional cloud instantaneously released in a uniform stream, which has been analysed mathematically and by computation of discrete vortex filaments by Rottman & Simpson (1984) and Rottman, Simpson & Stansby (1987). They have modelled the cloud as a bounding vortex sheet separating two regions of irrotational flow where the velocity potentials ϕ_j for the internal flow (the cloud itself), and ϕ_e for the external stream are defined. Their solutions show that when a circular cylindrical cloud is released, it begins to be deformed by the external flow and that this deformation is proportional to t^2 in the early stages of the deformation.

However, this deformation is symmetrical with respect to the normal to the free-stream direction and the centroid of the cloud does not move at $O(t^2)$.

The deformation of the interface can be derived by applying the initial conditions

$$\gamma(\theta, t = 0) = -2U_\infty \sin\theta, \tag{1}$$

and

$$u_s(\theta, t = 0) = -U_\infty \sin\theta \tag{2}$$

to the vortex-sheet equation for two-dimensional flows (Moore 1978),

$$\frac{\partial \gamma}{\partial t} + \frac{\partial}{\partial s}(u_s \gamma) = 0, \tag{3}$$

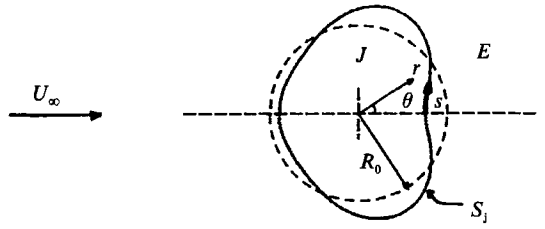

FIGURE 2. Nomenclature for the two-dimensional vortex-sheet model.

where s is the arclength of the vortex-sheet, γ its strength, and u_s is the average speed of the flow across the layer (assuming uniform density for simplicity), i.e.

$$u_s = \frac{1}{2}\left[\frac{\partial(\phi_e|_{f=0})}{\partial s} + \frac{\partial(\phi_j|_{f=0})}{\partial s}\right], \tag{4}$$

where $f(r,\theta,t) = 0$ defines the position of the vortex sheet.

Expanding $\gamma(\theta,t)$, $u_s(\theta,t)$ and $R(\theta,t)$ (see figure 2) in Taylor expansions with respect to t, one can directly evaluate derivatives of any order with respect to t at $t = 0$ for γ, u_s and $R(\theta,t)$. This gives

$$R(\theta,t) = R_0 - \left[\frac{1}{2}\frac{U_\infty^2}{R_0}\cos(2\theta)\right]t^2 + \left[\frac{1}{6}\frac{U_\infty^3}{R_0^2}\{3\cos(3\theta) - \cos\theta\}\right]t^3 + O(t^4). \tag{5}$$

This expression shows that the centroid of the cloud *does* move at $O(t^3)$.

Using the assumption that the jet flow can be parameterized with respect to time in this region of the flow, one substitutes t for $2z/U_j$ (elements of the vortex-sheet travel at half speed) in (5). Scaling with respect to U_j and R_0, it can be seen that Chang-Lu's approximation predicts the following deformation for the jet, for small values of $\lambda = U_\infty/U_j$:

$$R(\theta,z) = 1 - [2z^2(\cos 2\theta)]\lambda^2 - [\tfrac{4}{3}z^3(3\cos 3\theta - \cos\theta)]\lambda^3 + O(\lambda^4). \tag{6}$$

This implies that the centroid of the jet,

$$\bar{X} = \int_A r\cos(\theta)\,\mathrm{d}A/A$$

(A = cross-sectional area) moves downstream in proportion to z^3.

3. The three-dimensional vortex-sheet model

The solution presented in §2 was derived on the basis of an intuitive assumption about the equivalence of the spatial and temporal growth of the jet. In this section, a fully three-dimensional inviscid model is presented that does not require this assumption. The solution for this new model shows that the basis of the two-dimensional approach is fundamentally incorrect.

Considering the three-dimensional vortex-sheet model for strong jets (see figure 3), where $\lambda = U_\infty/U_j$ is a small parameter, one could argue that the process of convection of longitudinal vorticity changes the strength of the bounding sheet as the fluid moves away from the nozzle, leading to the same kind of distortion as predicted by the two-dimensional approximation.

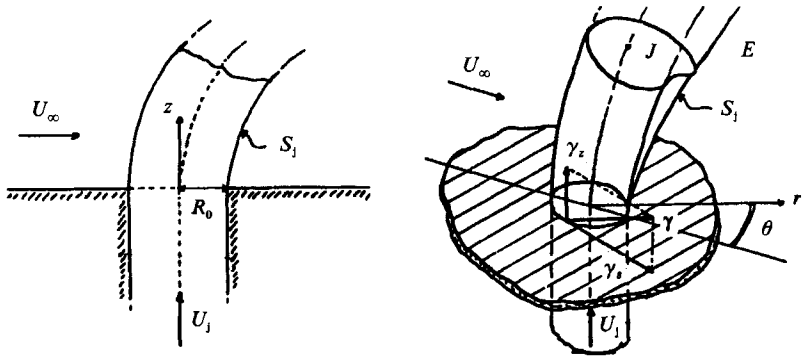

FIGURE 3. Nomenclature for the three-dimensional vortex-sheet model.

This argument, however, is not supported by a complete analysis: the interaction between the jet and the stream affects the flow within the issuing pipe. Consequently, it is not correct to assume that the flow issuing out of the nozzle is uniform (as is assumed in the two-dimensional approximation). A non-uniform distribution of the vertical component of the velocity at the nozzle due to this interaction would cause an initially planar ring of fluid in the vortex sheet to not remain planar as it moves upwards along the jet. This invalidates the approximation $R(\theta, z) = R(\theta, t)$, where $t = 2z/U_j$. The non-uniform flow within the issuing pipe would also induce a distribution of the transverse velocity, u_s, different from that shown in (2).

Furthermore, the two-dimensional approximation does not take into account the effects of the initial azimuthal component of vorticity present in the jet, which is typically much stronger than the longitudinal one for the case of strong jets. The strength of the three-dimensional vortex sheet is a vector γ, which can be split into two components. The first is due to the vorticity in the longitudinal direction, and can be approximated by its vertical component, γ_z, in the near field of the flow. The second is due to the strong transverse vorticity, and it can be approximated by the azimuthal component, γ_s, also in the near field of the flow. Using the vorticity equation, the following expression for the strength γ of the vortex sheet can be derived:

$$\frac{\partial \gamma}{\partial t} + (\boldsymbol{u}_v \cdot \nabla)\gamma = (\gamma \cdot \nabla)\boldsymbol{u}_v - \gamma(\nabla \cdot \boldsymbol{u}_v), \tag{7}$$

where $\boldsymbol{u}_v$ is the velocity of fluid elements in the vortex sheet, and $\nabla = \tilde{\partial}/\partial s\,\hat{\boldsymbol{s}} + \partial/\partial z\,\hat{\boldsymbol{z}}$, where $\hat{\boldsymbol{s}}$ and $\hat{\boldsymbol{z}}$ are unit vectors in the orthogonal directions s and z, which are tangent to the surface of the vortex sheet. Expression (7) is obtained by integrating the vorticity equation across the vortex sheet.

The z-component of (7) is

$$u_z \frac{\partial \gamma_z}{\partial z} + \frac{\partial}{\partial s}(u_s \gamma_z) = \frac{\partial u_z}{\partial s}\gamma_s, \tag{8}$$

where u_s is defined as in (4) and, similarly to (4),

$$u_z = \frac{1}{2}\left[\frac{\partial \phi_e|_{f=0}}{\partial z} + \frac{\partial \phi_j|_{f=0}}{\partial z}\right]. \tag{9}$$

Comparing (8) with (3), one can readily see that the three-dimensional vortex-sheet equation provides an extra term that has a significant effect on the longitudinal

strength γ_z along z. According to (8), even small variations in u_z can produce significant contributions to $\partial\gamma_z/\partial z$ because of the large values of γ_s.

The material derivative for γ_z is a function not only of the rate of stretching of the vortex sheet in the azimuthal direction ($\partial/\partial s(u_s\gamma_z)$), as assumed in the two-dimensional model, but also of the rate at which fluid elements rotate as they travel upwards along the vortex-sheet ($\gamma_s\,\partial u_z/\partial s$).

This rotation changes the direction of γ, transferring vorticity from the azimuthal direction to the vertical one or vice versa. This induces a non-uniform distribution of u_z over the cross-sectional area of the jet, affecting the rate of change of γ_z.

In order to take into account the above-mentioned effects, asymptotic solutions in integral powers of the small parameter $\lambda = U_\infty/U_j$ were obtained for the three-dimensional vortex-sheet model, where the condition of uniform flow was required not at the exit of the pipe but, instead, within it, far from the exit. The boundary-value problem is established in terms of the velocity potentials ϕ_j and ϕ_e for the internal and the external regions, respectively, and is summarized as follows (with reference to figure 3; scaling all variables with respect to U_j, R_0 and ρ, and assuming uniform density for simplicity):

$$\left.\begin{aligned}
&\nabla^2\phi_j = 0; \quad p_j + \tfrac{1}{2}(\nabla\phi_j)^2 = \tfrac{1}{2} + P \quad \text{in } J,\\
&\nabla^2\phi_e = 0; \quad p_e + \tfrac{1}{2}(\nabla\phi_e)^2 = \tfrac{1}{2}\lambda^2 \quad \text{in } E,\\
&\frac{Df}{Dt} = 0 \quad \text{on } f = 0, \quad \text{where } f(r,\theta,z) = 0 \quad \text{defines } S_j,\\
&p_j = p_e \quad \text{on } S_j,\\
&\frac{\partial\phi_j}{\partial r} = 0 \quad \text{on } r = 1, \quad z < 0,\\
&\frac{\partial\phi_e}{\partial z} = 0 \quad \text{on } z = 0, \quad r > 1,\\
&\nabla\phi_e \to \boldsymbol{\lambda}, \quad p_e \to 0 \quad \text{as } r \to \infty, \quad \text{where } \boldsymbol{\lambda} = \boldsymbol{U}_\infty/|\boldsymbol{U}_j|,\\
&\nabla\phi_j \to \hat{z}, \quad p_j \to P \quad \text{as } z \to -\infty, \quad \text{where } P = \text{const.}
\end{aligned}\right\} \tag{10a}$$

The solutions obtained for each order of λ are

$$O(1): \quad \phi_j^{(0)} = z; \quad p_j^{(0)} = 0; \quad \phi_e^{(0)} = 0; \quad p_e^{(0)} = 0; \quad R^{(0)} = 1, \tag{10b}$$

$$O(\lambda): \quad \phi_j^{(1)} = 0; \quad p_j^{(1)} = 0; \quad \phi_e^{(1)} = \left(r + \frac{1}{r}\right)\cos\theta; \quad p_e^{(1)} = 0; \quad R^{(1)} = 0, \tag{10c}$$

$$\left.\begin{aligned}
O(\lambda^2): \quad &\phi^{(2)}_{j(z>0)} = F_2(r,z)\cos 2\theta; \quad \phi^{(2)}_{j(z<0)} = G_2(r,z)\cos 2\theta;\\
&p^{(2)}_{j(z>0)} = -\left[\frac{\partial F_2}{\partial z}\cos 2\theta + \frac{1}{2}\right]; \quad p^{(2)}_{j(z<0)} = -\left[\frac{\partial G_2}{\partial z}\cos 2\theta + \frac{1}{2}\right];\\
&\phi_e^{(2)} = 0; \quad p_e^{(2)} = \frac{1}{r^2}\cos 2\theta - \frac{1}{2r^4};\\
&R^{(2)} = -\left\{z^2 - 2C_2 z - \sum_{n=1}^{\infty} A_n J_3(\sigma_n)\left[\exp(-\sigma_n z) - 1\right]\right\}\cos 2\theta.
\end{aligned}\right\} \tag{10d}$$

Here

$$F_2 = (C_2 - z)\,r^2 + \sum_{n=1}^{\infty} A_n J_2(\sigma_n r)\exp(-\sigma_n z),$$

n	1	2	3	4	5	6	...	99	100
A_n	−0.0611	0.0236	−0.0127	0.0080	−0.0055	0.0040	...	-2.54×10^{-5}	2.50×10^{-5}
B_n	−0.3892	0.0467	−0.0194	0.0107	−0.0068	0.0047	...	-2.42×10^{-6}	1.56×10^{-6}

TABLE 1. Coefficients A_n and B_n

and
$$G_2 = \sum_{n=1}^{\infty} B_n J_2(\tau_n r)\exp(\tau_n z),$$

where σ_n are zeros of J_2, τ_n are zeros of J_2', and A_n, B_n and C_2 are constants which can be determined from the boundary and matching conditions. The matching conditions across $z = 0$ require
$$C_2 = \sum_{n=1}^{\infty} B_n J_2(\tau_n) = \frac{1}{2}\sum_{n=1}^{\infty} A_n \sigma_n J_3(\sigma_n)$$

(giving $C_2 \approx -0.2164$), and a few values for A_n and B_n are given in table 1.

The behaviour of the series A_n and B_n was investigated and compared with the convergent series $\Sigma_{n=1}^{\infty} 1/n^2$ up to 100 terms. The curves for A_n and B_n fall well below the curve for $\Sigma_{n=1}^{\infty} 1/n^2$, indicating a convergence rate of $o(N^{-2})$. In addition, on evaluating $\phi^{(2)}_{j(z>0)}(r, \theta = 0, z = 0)$ and $\phi^{(2)}_{j(z<0)}(r, \theta = 0, z = 0)$, it was found that these two functions converge as N increases, and at $N = 100$ no difference between them was detected. Similar results were found on evaluating $p^{(2)}_{j(z>0)}(r, \theta = 0, z = 0)$ and $p^{(2)}_{j(z<0)}(r, \theta = 0, z = 0)$.

$$O(\lambda^3): \quad \phi_j^{(3)} = 0; \quad p_j^{(3)} = 0; \quad \phi_e^{(3)} = 3F_3\cos 3\theta - F_1\cos\theta; \quad p_e^{(3)} = 0; \quad R^{(3)} = 0, \tag{10e}$$

where F_3 and F_1 are non-separable functions of r and z, satisfying the boundary-value problem generated for the plane (z, r).

Thus, the three-dimensional vortex-sheet model gives
$$R(\theta, z) = 1 - \lambda^2\left[z^2 - 2C_2 z - \sum_{n=1}^{\infty} A_n J_3(\sigma_n)(\exp(-\sigma_n z) - 1\right]\cos 2\theta + O(\lambda^4). \tag{11}$$

4. Comparing the solutions for the two inviscid vortex-sheet models

Comparing (11), which gives the deformation according to the fully three-dimensional model, with (6), which gives the deformation according to the two-dimensional approximation, it can be seen that, even at second order, there is a marked difference between the results. According to (11), the deformation at $O(\lambda^2)$ is symmetric and has three components: one proportional to z^2, also predicted by the two-dimensional model but with a constant of proportionality only one half of that predicted by the latter (because of the greater pressure gradient needed to accelerate the external two-dimensional flow in the two-dimensional time-dependent model); a second component which is linear in z; and a third one which decays exponentially with z. The last two components of this deformation are not present in the two-dimensional model. The linear component of the deformation is caused by a non-zero distribution of the radial component of the velocity of the jet at the exit. The pressure field inside the pipe is not uniform, and the velocity field associated with it is also non-uniform.

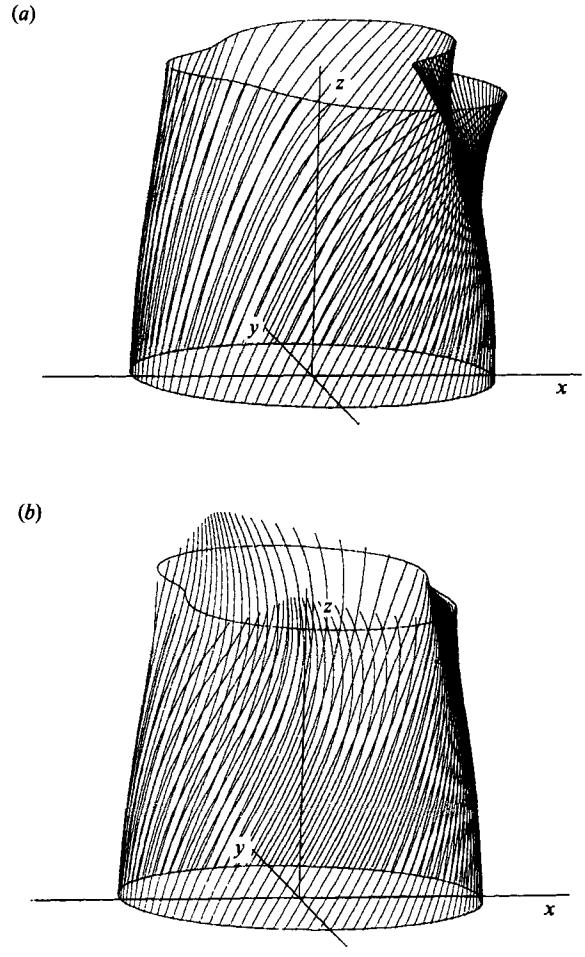

FIGURE 4. Streamline pattern on the vortex sheet according to (*a*) the two-dimensional and (*b*) the three-dimensional vortex-sheet model.

The exponential term in the expression for $\phi_j^{(2)}$ is identified as an 'exit effect' and ensures that the matching conditions at the exit are fulfilled; the radial component of the jet velocity at the exit is indeed zero at $r = 1$. Expanding the exponential term of $(10d)$ in Taylor series about $z = 0$, it can be seen that the linear term of this expansion is $\Sigma_{n=1}^{\infty} A_n \sigma_n J_3(\sigma_n) z$, which cancels with the linear term $-2C_2 z$, since the matching conditions across the surface $z = 0$ require $C_2 = \frac{1}{2}\Sigma_{n=1}^{\infty} A_n \sigma_n J_3(\sigma_n)$. Thus, the solution at $O(\lambda^2)$ does lead to $\partial R^{(2)}/\partial z = 0$ at $z = 0$.

The two-dimensional model assumes that the velocity field is uniform at the exit of the pipe. However, the three-dimensional model shows a deflection of the streamlines within the pipe at $O(\lambda^2)$. Because of the symmetrical external pressure field the streamlines of the flow within the pipe are deflected towards the y-axis and away from the x-axis. Figure 4 shows the streamline pattern on the bounding vortex sheet according to each of the two models. Therefore, the vertical velocity component at the exit of the pipe decreases towards the pipe wall along the x-axis and increases symmetrically towards the pipe wall along the y-axis. The radial component is negative along the x-axis and positive along the y-axis, being zero at

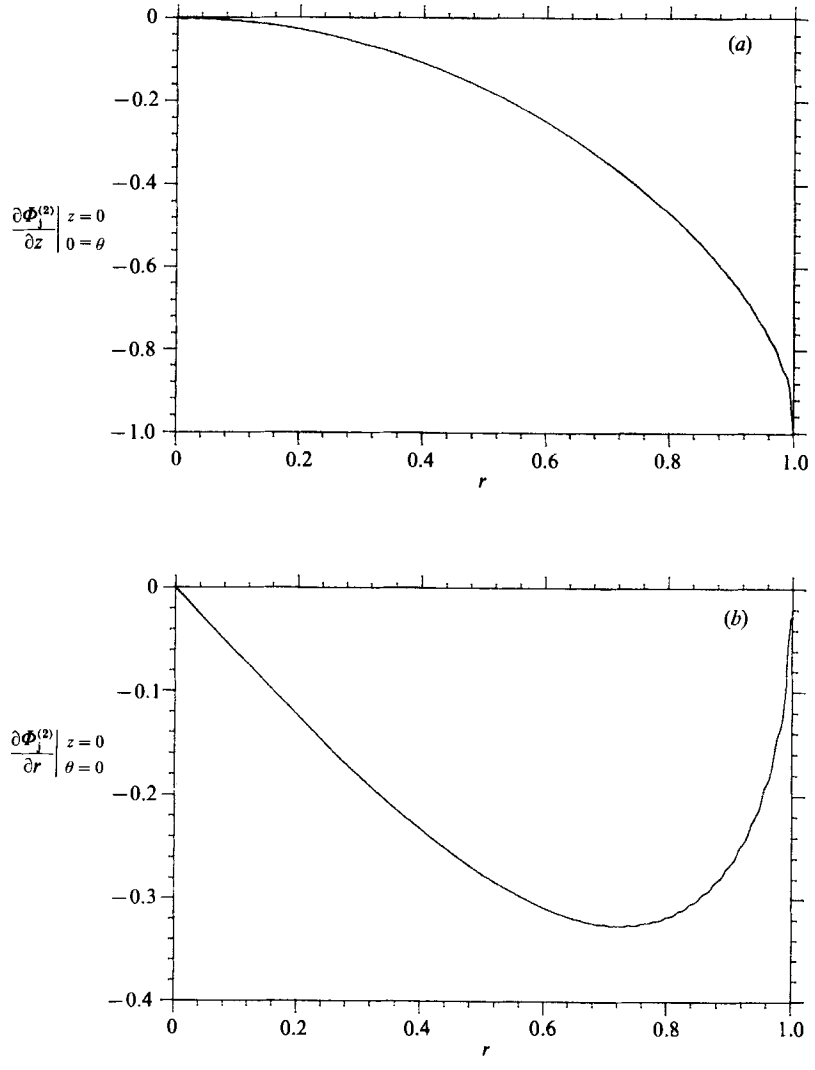

FIGURE 5. Corrections for (*a*) the vertical velocity and (*b*) the radial velocity, at order λ^2.

$r = 1$. Figure 5 shows these velocity components at $z = 0$ for $\theta = 0$; for $\theta = \frac{1}{2}\pi$ these distributions are symmetrically equivalent to those shown in figure 5.

However, the most remarkable difference between these solutions is found at the third-order term: the three-dimensional vortex-sheet solution does not describe any deformation at $O(\lambda^3)$. The effects of the non-uniform flow induced by the jet within the pipe, and of the transport of azimuthal vorticity which were described in the first paragraphs of §3, completely change the deformation at this order. They inhibit the distortion induced by the convection of vertical vorticity from the upwind side to the downwind side of the vortex sheet which is predicted by the two-dimensional approach. It can be seen from (10*b–e*) that, owing to these effects, the differences in u_s and u_z at $z = 0$, compared with the distributions assumed in the two-dimensional model, are of order λ^2.

The trajectory of an initially planar ring of fluid in the vortex sheet according to

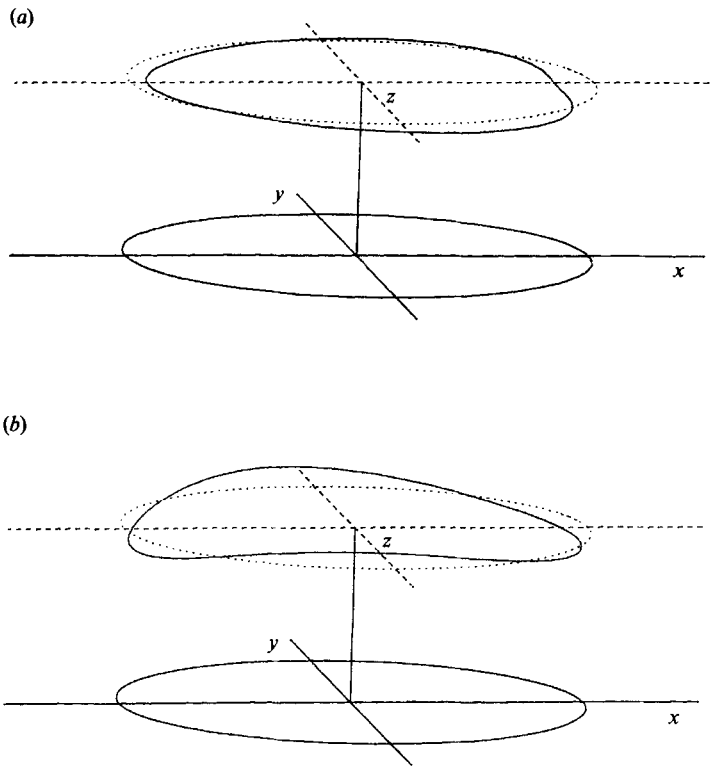

FIGURE 6. Trajectory of an initially planar ring of fluid in the vortex sheet according to (*a*) the two-dimensional and (*b*) the three-dimensional vortex-sheet model.

each of the two models is shown in figure 6, for solutions including terms up to $O(\lambda^3)$. Chang-Lu's approach assumes that the ring remains planar as it moves along its trajectory and the concentration of vertical vorticity in the downwind side of the vortex sheet (by means of convection) induces the non-symmetrical distortion of the jet. The three-dimensional model, however, shows a non-planar deformation of this ring, due to the concentration of the azimuthal component of vorticity. The lateral sections of the vortex lines (which are also material lines in this inviscid approach) move faster in the vertical direction than their upwind and downwind sections. This mechanism tilts the vorticity vector by different amounts along the vortex sheet, transferring vorticity from the azimuthal direction to the z-direction on the upwind side of the vortex sheet, and from the z-direction to the azimuthal direction on the downwind side. For an issuing angle of 90°, the processes of convection and transference of vorticity from one direction to another cancel each other and the net distributions of γ_s and γ_z remain symmetrical. The distortion of the jet is therefore also symmetrical.

As a matter of fact, by inspecting the expanded forms of the Bernoulli and the internal-boundary-condition equations, it can be seen that $\phi_j^{(n)}$ and $p_j^{(n)}$ are zero for n odd, if $\phi_j^{(i)}$ and $p_j^{(i)}$ are also zero, for i odd $< n$. Therefore, it is found that the deformation of the vortex sheet is always symmetric no matter to what order of λ one evaluates $R(\theta, z)$! This is so because of the symmetry of the boundary conditions. If this symmetry is altered in any way, for instance by the introduction of a vertical component in the free-stream velocity, non-symmetric components of deformation

similar to those predicted by the two-dimensional model will be present in the asymptotic solution (this can be accomplished by the insertion of another small parameter which represents this vertical component of the free-stream velocity in the previous boundary-value problem, determining an asymptotic solution in integral powers of two small parameters).

Previous work by Maskell & Spence (1959), where jet flaps of finite span (thin jets issuing at small angles from the trailing edge of wings of finite span) have been modelled as potential flows bounded by vortex sheets, has predicted deflections for the jet which are greater than the values that would be obtained with the above-mentioned model. In this case, however, the symmetry of the problem is broken not only by the coflowing component of the external flow, but also by the circulation produced around the wing. The difference between the strength of the bounding vortex sheet at the upwind side of the jet and at its downwind side is increased by this latter mechanism (different fluxes of transverse vorticity come from the top and from the bottom of the wing). This allows for the existence of a pressure discontinuity across the thin jet (in fact, the jet is represented by a sheet of vortices *and* doublets). However, the deflection of jets issuing at large angles to the stream from pipes or plane walls cannot be explained by these mechanisms. In these cases there would be no inviscid mechanism to produce a transverse circulation large enough to explain the deflection of the jet. At right angles to the flow, in particular, the strength of the vortex sheet would be the same at both sides of the jet.

This analysis has shown that Chang-Lu's two-dimensional vortex-sheet model is an incorrect approximation for the near field of the jet, in that it does not satisfy the boundary conditions or the three-dimensional equations that govern the jet behaviour in this region. It is quite widely used to model the far field of the jet; however, if it is rectified to allow for the three-dimensionality of the near field, the essential features of the initial development of the jet are not reproduced. In particular, the jet does not move downwind. The displacements of the jet are symmetric about the plane $y = 0$. Furthermore, the generation of the vorticity present in the bounding vortex sheet is not considered nor explained by the two-dimensional time-dependent model.

Only a full three-dimensional analysis includes the tangential pressure gradients along the inner pipe walls that (as shown by Morton 1984) are necessary for the generation of vorticity γ_z. The three-dimensional analysis also shows that the vorticity disturbances superimposed on the unperturbed component $\gamma_s^{(0)}$ (convected along the pipe boundary layer) are generated in the region near the pipe exit by the pressure distribution along the pipe wall, which is induced by the presence of the crossflow.

The fact that the three-dimensional inviscid vortex-sheet model cannot reproduce the streamwise deflection of the jet suggests that the main mechanism responsible for this deflection may be the addition of streamwise momentum due to viscous processes such as entrainment (and not by 'pressure drag' as assumed in many of the referenced integral models).

Taylor in his 1958 paper on the flow induced by jets recalls that 'The sudden change in flow velocity at the cut in the theoretical flow which idealizes the action of the jet on the surrounding fluid seems to be more nearly related to a sheet of sinks than to a sheet of vortices'.

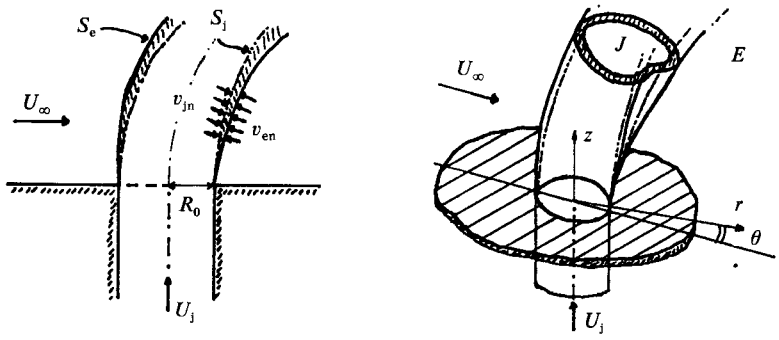

FIGURE 7. Nomenclature for the entraining vortex-sheet model.

5. A three-dimensional model that considers turbulent entrainment

By extending the inviscid three-dimensional model derived in §3 to allow for turbulent entrainment, a new study of the effects of viscosity is presented in this section. This study is carried out by deriving asymptotic solutions for a model for the near field of the jet that includes the effects of turbulent entrainment.

The near field of the jet can be seen as a mixing layer of small thickness separating two regions of irrotational flow: the potential core and the external stream (see figure 7). The mixing layer grows thicker as z increases as a result of turbulent entrainment. Assuming that the thickness of this mixing layer, δ, is proportional to the entrainment rate, this layer can be regarded as a thin free shear layer that entrains fluid from the surrounding flow. Neglecting the effects of the curvature of this 'entraining vortex sheet', it can be assumed that the entrainment velocity v_{en} is proportional to the local strength, $|\gamma|$, of the vortex sheet. This assumption is in agreement with Tollmien's analysis for plane turbulent compound shear layers (Rajaratnam 1976), where the entrainment velocity is found to be proportional to the local velocity excess.

For small ratios $\lambda = U_\infty/U_j$, the entrainment coefficient for a free jet in a still environment, which has been extensively analysed in the literature (e.g. Pai 1954; Abramovich 1963; Rajaratnam 1976), can be assumed to be the constant of proportionality between v_{en} and $|\gamma|$. Moreover, it can be assumed that the entrainment coefficient is a small parameter $\epsilon \to 0$, and an asymptotic solution in integral powers of two small parameters (λ and ϵ) can be sought. From experimental data (Rajaratnam 1976) it is found that the entrainment coefficient for circular jets varies only slightly with z in the developing region of the jet, supporting the following relation:

$$v_{en} = \epsilon(\gamma_s^2 + \gamma_z^2)^{\frac{1}{2}} + O(\epsilon^2), \tag{12}$$

where

$$\gamma_s = \left[\frac{1}{R_j}\frac{\partial \phi_j}{\partial \theta}\bigg|_{f_j=0} - \frac{1}{R_e}\frac{\partial \phi_e}{\partial \theta}\bigg|_{f_e=0}\right], \quad \gamma_z = \left[\frac{\partial \phi_j}{\partial z}\bigg|_{f_j=0} - \frac{\partial \phi_e}{\partial z}\bigg|_{f_e=0}\right]. \tag{13}$$

The 'internal entrainment velocity', v_{jn}, is a function of the internal spreading angle of the shear layer, which is determined by the distribution of the momentum flux within the layer. Nevertheless, a constant $k = O(1)$ can be defined relating the leading-order terms for v_{en} and v_{jn}:

$$v_{en} = \epsilon|\gamma| + O(\epsilon^2), \quad v_{jn} = \epsilon k|\gamma| + O(\epsilon^2). \tag{14}$$

Applying the continuity equation to the flow within the mixing layer and making use of (14), an equation for mass conservation in the mixing layer can be derived for the near field of the circular jet (in cylindrical coordinates):

$$\frac{\partial}{\partial\theta}[u_\theta(R_e-R_j)]+\frac{\partial}{\partial z}\left[u_z\left(\frac{R_e^2-R_j^2}{2}\right)\right]=\epsilon|\gamma|\left\{\left[R_e^2+\left(\frac{\partial R_e}{\partial\theta}\right)^2\right]^{\frac{1}{2}}+k\left[R_j^2+\left(\frac{\partial R_j}{\partial\theta}\right)^2\right]^{\frac{1}{2}}\right\}+O(\epsilon^2), \tag{15}$$

where u_θ and u_z are the average velocities for the flow in the mixing layer in the azimuthal and vertical directions, respectively, i.e.

$$u_\theta=\frac{1}{2}\left[\frac{1}{R_j}\frac{\partial\phi_j}{\partial\theta}\bigg|_{f_j=0}+\frac{1}{R_e}\frac{\partial\phi_e}{\partial\theta}\bigg|_{f_e=0}\right],\quad u_z=\frac{1}{2}\left[\frac{\partial\phi_j}{\partial z}\bigg|_{f_j=0}+\frac{\partial\phi_e}{\partial z}\bigg|_{f_e=0}\right]. \tag{16}$$

R_e and R_j are the external and the internal radii of the mixing layer, respectively. Here the mixing layer is defined as the region of rotational flow. Shear-layer approximations for the momentum equations (Hinze 1959) indicate that the pressure change across the mixing layer is of order δ^2. Since $\delta=O(\epsilon)$, the following boundary-value problem incorporating these assumptions can be formulated (with reference to figure 7; variables are scaled with respect to U_j, R_0 and ρ, and uniform density is assumed for simplicity):

$$\left.\begin{aligned}
&\nabla^2\phi_j=0;\quad p_j+\tfrac{1}{2}(\nabla\phi_j)^2=\tfrac{1}{2}+P,\quad \text{in } J,\\
&\nabla^2\phi_e=0;\quad p_e+\tfrac{1}{2}(\nabla\phi_e)^2=\tfrac{1}{2}\lambda^2\quad \text{in } E,\\
&\nabla\phi_e\frac{\nabla f_e}{|\nabla f_e|}=-\epsilon|\gamma|+O(\epsilon^2)\quad \text{on } f=0,\quad \text{where } S_e: f_e(r,\theta,z)=0,\\
&\nabla\phi_j\frac{\nabla f_j}{|\nabla f_j|}=\epsilon k|\gamma|+O(\epsilon^2)\quad \text{on } f=0,\quad \text{where } S_j: f_j(r,\theta,z)=0,\\
&p_j(r=R_j,\theta,z)-p_e(r=R_e,\theta,z)=O(\epsilon^2),\\
&\frac{\partial\phi_j}{\partial r}=0\quad \text{on } r=1,\quad z<0,\\
&\frac{\partial\phi_e}{\partial z}=0\quad \text{on } z=0,\quad r>1,\\
&\nabla\phi_e\to\boldsymbol{\lambda},\quad p_e\to 0\quad \text{as } r\to\infty,\quad \text{where } \boldsymbol{\lambda}=\boldsymbol{U}_\infty/|\boldsymbol{U}_j|\\
&\nabla\phi_j\to\hat{\boldsymbol{z}},\quad p_j\to P,\quad \text{as } z\to-\infty,\quad \text{where } P=\text{const.},\\
&+\text{equation (15)}.
\end{aligned}\right\} \tag{17a}$$

The solutions obtained for each order of magnitude are

$$O(1):\quad \phi_j^{(0)}=z;\quad p_j^{(0)}=0;\quad \phi_e^{(0)}=0;\quad p_e^{(0)}=0;\quad R_j^{(0)}=R_e^{(0)}=1, \tag{17b}$$

$$\left.\begin{aligned}
O(\lambda\epsilon^0):\quad &\phi_j^{(1,0)}=0;\quad p_j^{(1,0)}=0;\quad \phi_e^{(1,0)}=\left(r+\frac{1}{r}\right)\cos\theta;\\
&p_e^{(1,0)}=0;\quad R_j^{(1,0)}=R_e^{(1,0)}=0,
\end{aligned}\right\} \tag{17c}$$

$$\left.\begin{aligned}
O(\lambda^0\epsilon):\quad &\phi_j^{(0,1)}=0;\quad p_j^{(0,1)}=0;\quad \phi_e^{(0,1)}=-\ln r;\quad p_e^{(0,1)}=0;\\
&R_j^{(0,1)}=-kz;\quad R_e^{(0,1)}=(2+k)z,
\end{aligned}\right\} \tag{17d}$$

$$\left.\begin{aligned}
O(\lambda\epsilon):\quad &\phi_j^{(1,1)}=0;\quad p_j^{(1,1)}=0;\quad p_e^{(1,1)}=\left(\frac{1}{r}-\frac{1}{r^3}\right)\cos\theta\\
&\phi_e^{(1,1)}=\left[2(2+k)\frac{z}{r}+\sum_{n=1}^{\infty}A_{1n}J_1(\tau_{1n}r)\exp(-\tau_{1n}z)\right]\cos\theta;\\
&R_j^{(1,1)}=0;\quad R_e^{(1,1)}=2(1+k)z^2\cos\theta,
\end{aligned}\right\} \tag{17e}$$

where A_{1n} are constants determined from the boundary condition $\partial\phi_e^{(1,1)}/\partial z = 0$ at $z = 0$, and τ_{1n} are zeros of J_1'.

$O(\lambda^2\epsilon^0)$: Same expressions as in (10*d*), with $R_j^{(2,0)} = R_e^{(2,0)} = R^{(2)}$. (17*f*)

Thus, the three-dimensional entrainment model gives

$$R_j = 1-[kz]\,\epsilon-[Z(z)\cos 2\theta]\,\lambda^2+O(\epsilon^2,\lambda^3,\epsilon\lambda^2), \tag{18a}$$

and $$R_e = 1+[(2+k)\,z]\,\epsilon+[2(1+k)\,z^2\cos\theta]\,\epsilon\lambda-[Z(z)\cos 2\theta]\,\lambda^2+O(\epsilon^2,\lambda^3,\epsilon\lambda^2), \tag{18b}$$

where

$$Z(z) = z^2-2C_2\,z-\sum_{n=1}^{\infty} A_n\,J_3(\sigma_n)\,[\exp(-\sigma_n z)-1].$$

The mean radius $R = (R_e+R_j)/2$ is then

$$R(\theta,z) = 1+z\epsilon+[(1+k)\,z^2\cos\theta]\,\epsilon\lambda-[Z(z)\cos 2\theta]\,\lambda^2+O(\epsilon^2,\lambda^3,\epsilon\lambda^2). \tag{19}$$

Note that the position of the centroid is now $\bar{X} = \epsilon\lambda[(1+k)/2]\,z^2+O(\epsilon^2,\lambda^3,\epsilon\lambda^2)$.

6. Comparing the entraining vortex-sheet model with the inviscid models

Since these results are valid for layers of small thickness it can be assumed that in the regions of irrotational flow the velocity field induced by the vorticity present in the mixing layer is the same as if the vorticity was concentrated in a narrow strip at $r = R$: the 'entraining vortex sheet'. This allows for the comparison of (19) with (6) and (11). Doing so one finds, once again, marked differences among the results. The first non-symmetric term in the expression for the distortion according to an inviscid vortex model is of order λ^3 (Chang-Lu's model); a much higher order in λ than the non-symmetric term in (19): this term is of order $\lambda\epsilon$. The combined effects of the influx of fluid to the mixing layer due to turbulent entrainment, and its convection from the upwind side to the downwind side of the jet, lead to a higher rate of increase of δ on the downwind face. The centroid of the area determined by $R(\theta,z)$ then shifts downwind, by an amount which is, at first order, proportional to ϵ and λ. Turbulent entrainment also provides an influx of momentum from the external stream to the mixing layer, which contributes to the rate of stretching of fluid elements within this layer. From (10*b–e*) and (17*b–e*) it is seen that the change in $\partial u_z/\partial s$ and $\partial u_s/\partial s$ with respect to the distributions predicted by vortex-sheet models is also of order $\lambda\epsilon$.

The theoretical flows predicted by the inviscid vortex-sheet models are dependent only upon the strength of the vortex sheet. But now, the flow induced by the 'sinks' which were introduced in the vortex sheet has a significant effect on the movement of the initially planar rings of fluid discussed in §4. Vortex-sheet models cannot allow for these effects. The entraining fluid further increases the overall momentum of the mixing layer in the x-direction, increasing u_s as z increases. This leads to a more intensive concentration of γ_s at the downwind side of the jet. This stronger concentration is enough to compensate for the effects of vorticity transference from the azimuthal to the vertical direction, determining larger values for u_z in the downwind side of the jet. Figure 8 shows the trajectory of an initially planar ring of fluid in the boundary of the jet, according to the entraining vortex-sheet model.

General aspects of the topology of the flow along transverse planes are shown in figure 9. The pattern and the topology of these streamlines is quite different from that of the flow past a rigid bluff body. Figure 9(*a*) shows a single node at the downwind side of the jet contour in the near field. As the jet develops, two nodes

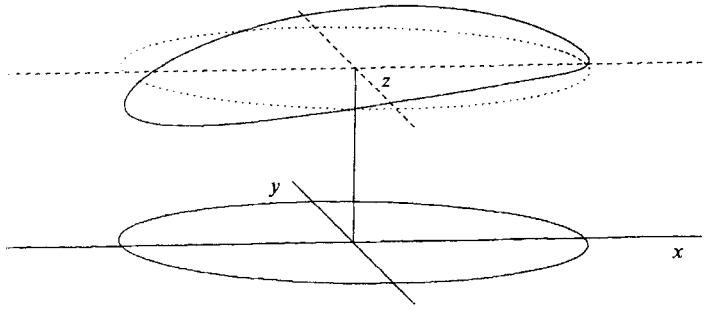

FIGURE 8. Trajectory of an initially planar ring of fluid in the boundary of the jet, according to the entraining vortex-sheet model. The downwind side of the ring moves faster because of the larger vertical velocity induced by the concentration of azimuthal vorticity in this region. This behaviour is also observed in the numerical simulation of the flow by Sykes, Lewellen & Parker (1986). Compare this with figure 6(*b*).

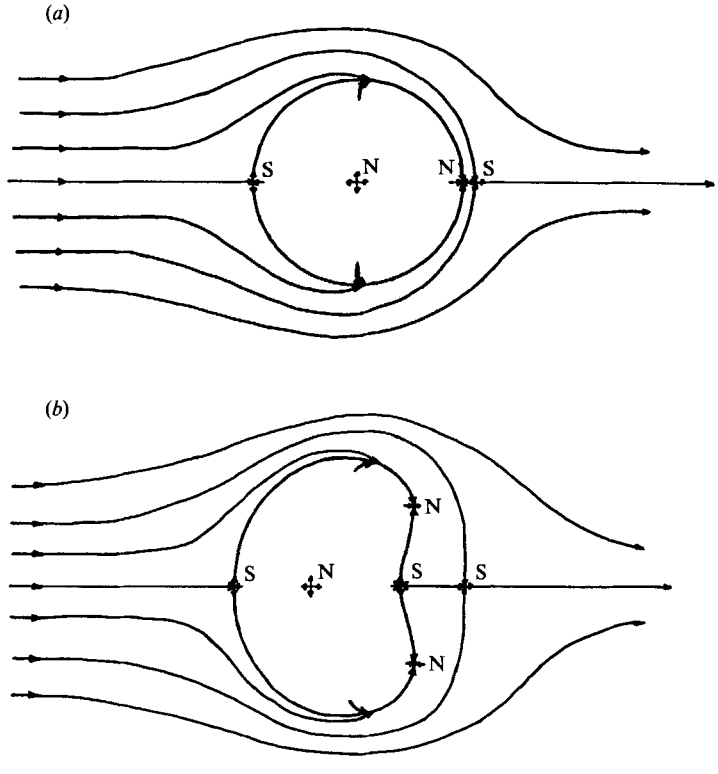

FIGURE 9. Topology of the flow over transversal planes: S denotes saddle points and N denotes node points. (*a*) refers to the initial region only; after the formation of the trailing vortices the topology should be more like (*b*).

appear on the downwind face, where vortices begin to roll up. The number of nodes and saddles satisfy the topological rules set out by Hunt *et al.* (1978). A detailed experimental study of the topology of the near field of jets has also been made by Foss (1980). The position of the rear 'stagnation' point is a function of λ/ϵ, which is shown graphically in figure 10. This variation of the location of the rear stagnation

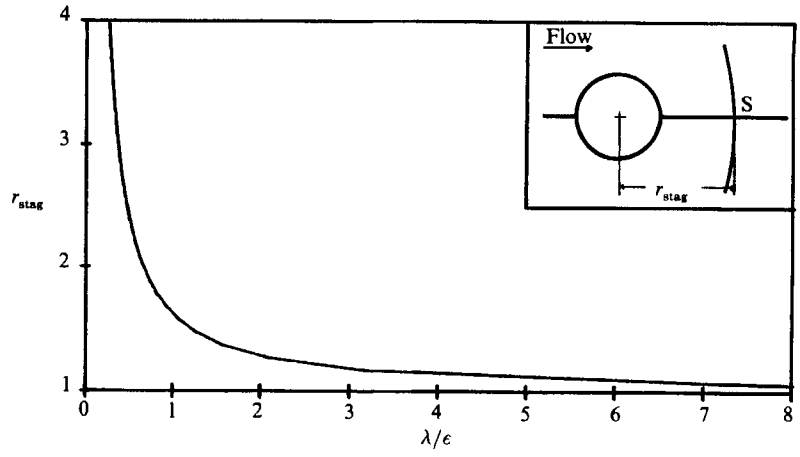

FIGURE 10. Position of the rear saddle as a function of λ/ϵ (jet stiffness/entrainment constant) according to the entraining vortex-sheet model, $R_0 = 1$).

point is similar to that obtained by the familiar calculation of a line source in a crossflow (Milne-Thomson 1960).

An important aspect of the asymptotic solutions for the entraining vortex-sheet model is the dependence of the initial distortion of the jet on the intensity of the turbulence present in the mixing layer. Different turbulence intensities for the incoming jet flow could induce different turbulent intensities in the mixing layer, determining different entrainment coefficients. The initial distortion of the jet would then also be a function of the level of turbulence present in the incoming flow. However, the intensity of turbulence in the mixing layer is very high (Andreopoulos & Rodi 1984 report measurements for $(\overline{u^2})^{\frac{1}{2}}/U_j$ up to 0.3 in the mixing layer) and so only high levels of turbulence in the incoming jet flow are likely to have significant effects on the initial developing of the flow. Turbulence in the oncoming crossflow is unlikely to have a considerable effect on the entrainment coefficient for strong jets because even relatively high turbulence intensities with rspect to U_∞ would be negligible with respect to the jet velocity U_j, meaning that velocity fluctuations induced by turbulence in the crossflow are very unlikely to be of the same order of magnitude as the velocity fluctuations in the mixing layer. Unfortunately, no systematic measurements of these effects have been found in the literature.

Another important result of the entraining vortex-sheet model is the prediction of the initial trajectory of the jet. According to (19) the position of the centroid of the cross-sections in the initial region is proportional to λ and z^2 (at the lowest order), leading to $z \propto \lambda^{-\frac{1}{2}} x^{\frac{1}{2}}$ (where x is the distance downstream from the jet exit); quite different from the behaviour in the far field. The assumption that the rolled up vortices control the far field leads to $z \propto \lambda^{-\frac{2}{3}} x^{\frac{1}{3}}$ (Broadwell & Breidental 1984) Experimental researchers seem to find $z \propto \lambda^{-a} x^b$, with a varying from 0.47 to 1 and b from 0.33 to 0.39. The reason for such a wide range of values for these coefficients is probably the fact that the evaluation of these constants is usually based on measurements taken from the whole range of the trajectory of the jet, disregarding the different behaviour suggested by the present results for the initial and far regions. Thus, the different ranges at which data are collected determine different values for these constants.

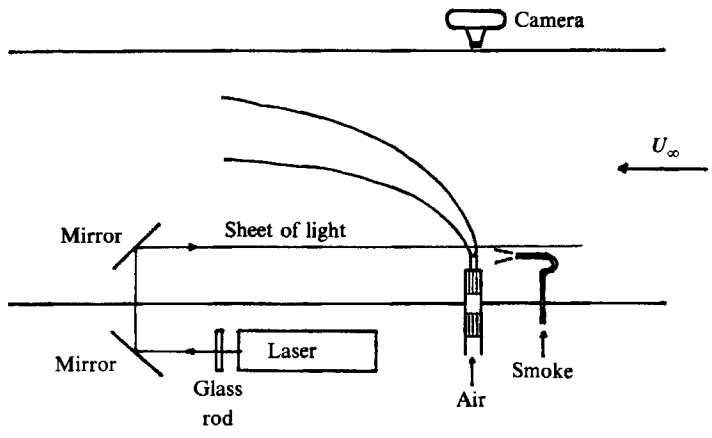

FIGURE 11. Experiment arrangement in the CUED smoke wind tunnel.

7. Comparison of the present models with experimental observation

Despite the vast literature on jets in crossflows, details of the flow near the jet exit have not been measured in the detail necessary to distinguish between different models. Thus, some new experiments were conducted in the Cambridge University Engineering Department's wind tunnel (described by Head & Bandyopadhyay 1981). The tunnel is specially designed for visualization studies of flows, using smoke as a tracer and laser illumination. The wind tunnel has a 1 m × 1 m square cross-section and is equipped with a 5 W laser generator. Air was supplied to the jet pipe by a flexible tube from a compressed air supply. Flow straighteners ensured a uniform velocity profile and low turbulence intensities (0.5%) at the pipe exit. This was placed 0.4 m from the tunnel wall, a distance sufficient to avoid boundary-layer effects. The jet was directed perpendicularly to the oncoming flow, which was uniform and contained weak small-scale turbulence with intensity of about 0.3%. A novel feature of the experiment was to introduce smoke with a 5 mm diameter smoke probe placed upstream from the pipe exit in such a position that a significant amount of the smoke delivered to the stream was entrained by the mixing layer in the initial region of the jet. The probe did not affect the jet flow. Transverse illumination was provided by a horizontal sheet of light, obtained by refracting the laser beam through a glass rod. This allowed for the visualization of the cross-sections of the jet and its potential core.

Positioning the sheet of light at different distances from the exit, cross-sections at different levels could be photographed from the transparent top wall of the tunnel. Figure 11 shows schematically the experimental set-up.

Mean and fluctuating velocity measurements were also made with a hot-wire anemometer around the initial region of the jet.

Using the photographs, the experimental jet cross-section can be compared with the predictions of each of the three models presented in §§2, 3 and 5. Cross-sections for an initial jet diameter $d_0 = 20$ mm, and jet and stream velocities $U_j = 9$ m/s, and $U_\infty = 0.9$ m/s ($\alpha = 10$, and $Re_j \approx 11400$) for two different distances from the exit ($z/d_0 = 3$, and $z/d_0 = 4$) are reproduced in figures 12 and 13, together with the corresponding predictions obtained with each of the three models. Hot-wire measurements of the external flow for a jet in the absence of a crossflow confirmed the value $\epsilon \approx 0.03$ reported by Rajaratnam (1976), and this was the value used for

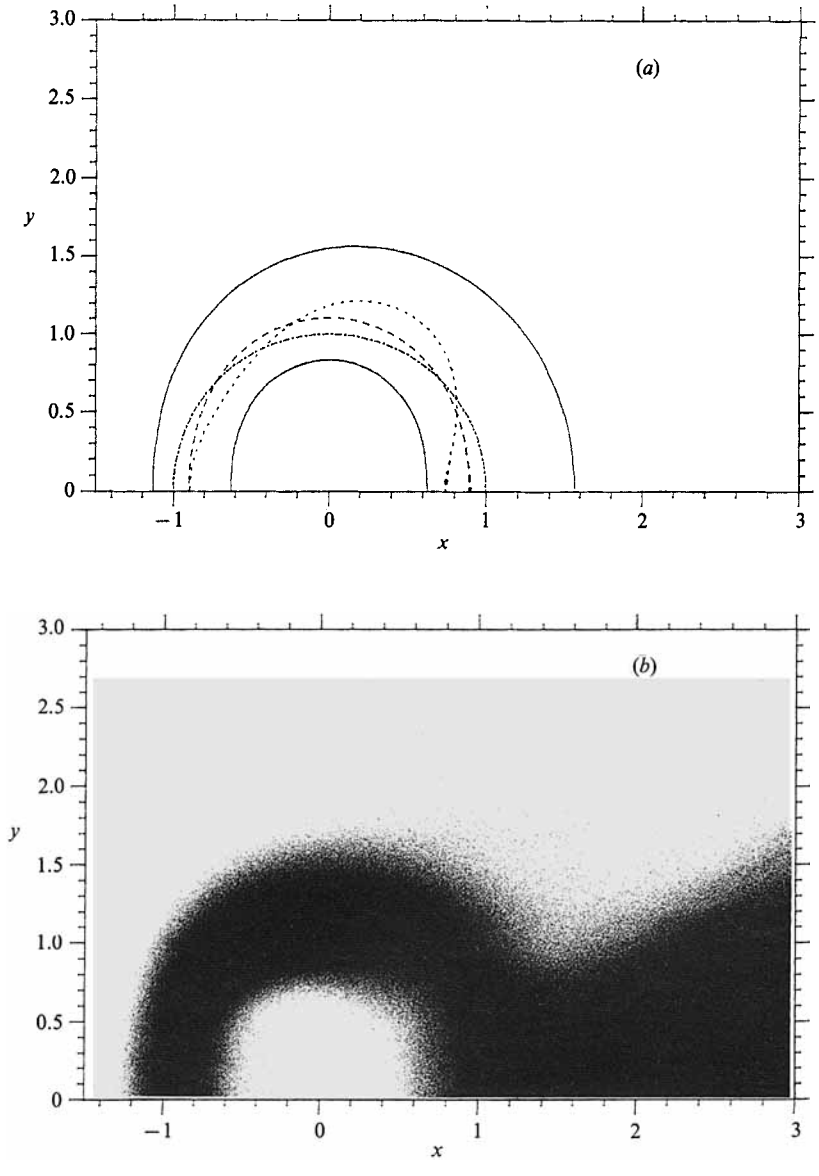

FIGURE 12. (*a*) Theoretical cross-section of the jet at $z/d_0 = 3$ for $\lambda = 0.1$ and $\epsilon = 0.03$. ···, 2D vortex-sheet model; – – –, 3D vortex-sheet model; ——, entraining model; –·–·, initial jet diameter. (*b*) Cross-section visualized by entrained smoke for $z/d_0 = 3$ and $\lambda = 0.1$.

ϵ in the theoretical calculations with the entraining vortex-sheet model. From experimental measurements, also reported by Rajaratnam (1976), it is found that $k \approx 3$ for turbulent axisymmetric jets, and this value was used in the theoretical calculations with the entraining vortex-sheet model.

The entraining vortex-sheet model seems to describe some of the important aspects of the flow: (i) no deflection of the potential core is predicted by the model; (ii) the jet expands laterally and in the downwind direction; (iii) the upwind side of the jet 'flattens' as the jet leaves the exit.

A quantitative measurement of the deformation of the jet in its initial region can

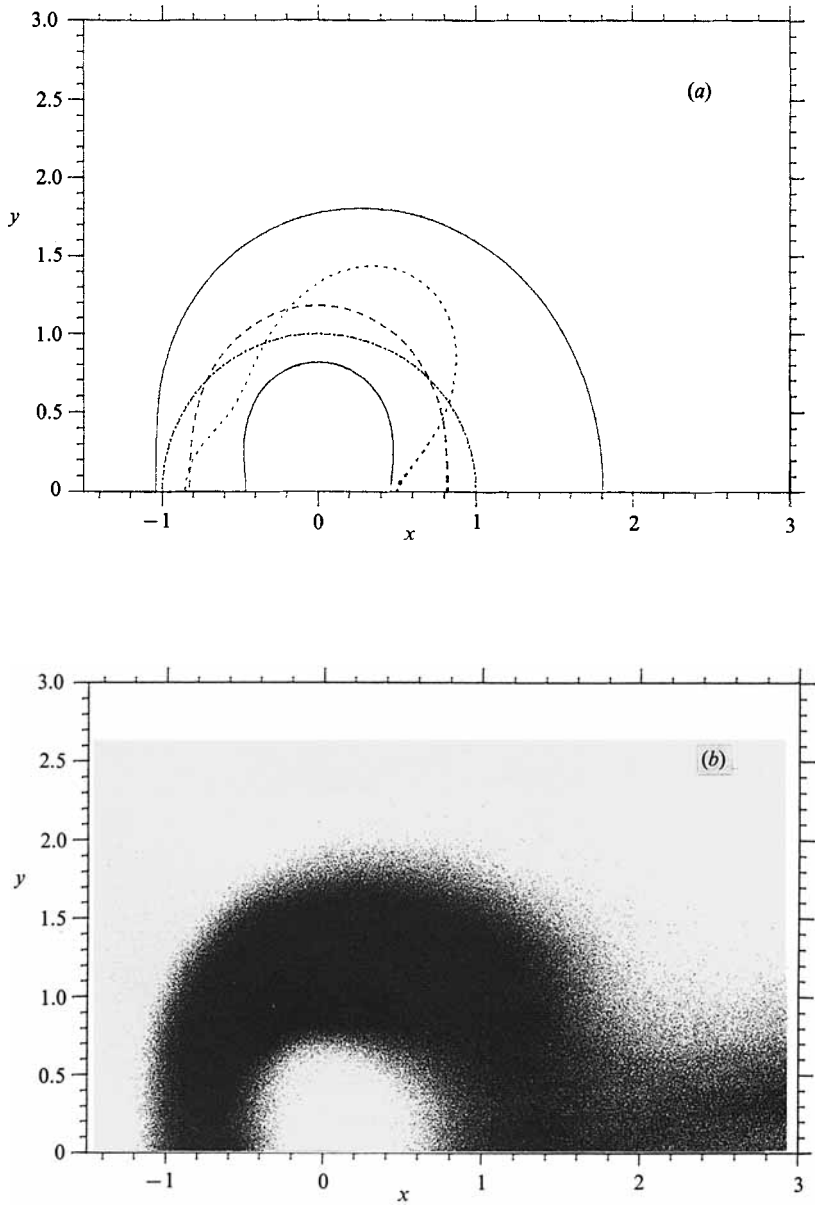

FIGURE 13. (*a*) Theoretical cross-section of the jet at $z/d_0 = 4$ for $\lambda = 0.1$ and $\epsilon = 0.03$. ···, 2D vortex-sheet model; – – –, 3D vortex-sheet model; ——, entraining model; –·–·, initial jet diameter. (*b*) Cross-section visualized by entrained smoke for $z/d_0 = 4$ and $\lambda = 0.1$.

be obtained from the positions, at each cross-section, of the outer and potential core boundaries, with respect to the axis at the centre of the initially circular cross-section (the centreline defined by the loci of maximum velocity obviously does not apply to this region of the flow). Figure 14 defines these characteristic lengths, which are the spanwise width of the jet (b_y), the position of the upwind boundary of the jet (b_{x1}), the position of the downwind boundary of the jet (b_{x2}), the streamwise and spanwise widths of the potential core (b_x^* and b_y^*, respectively), and the position along the x-axis where the maximum jet breadth occurs ($x_{\max}$). Four relevant ratios of these

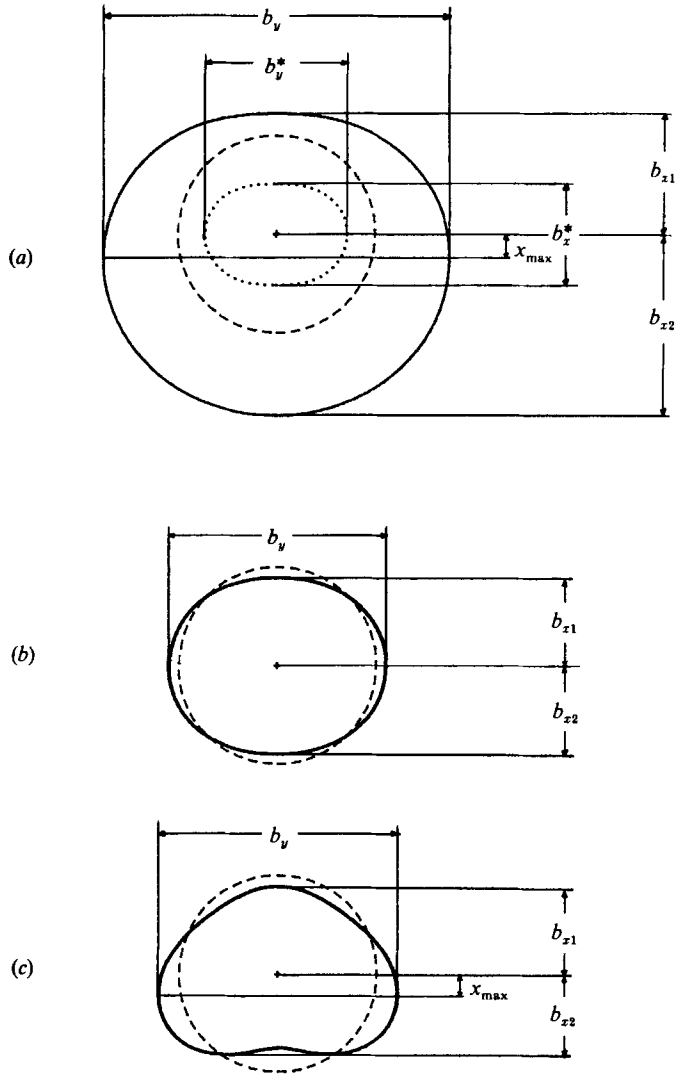

FIGURE 14. Characteristic lengths for the form of the cross-sections: (*a*) entraining model; (*b*) three-dimensional vortex-sheet model; (*c*) two-dimensional time-dependent vortex-sheet model.

lengths ($[b_{z1}+b_{z2}]/b_y$, b_{z1}/b_{z2}, b_z^*/b_y^*, and x_{max}/b_{z2}) are shown in figures 15 and 16, together with the predictions from each of the three models discussed herein. Figure 15 shows how all these models give the same initial prediction that, as the jet emerges, the spanwise width increases faster than the streamwise width (note that integral models do not account for this effect). Figure 16 shows that, as the jet travels along z, the streamwise thickness of the jet increases more rapidly on the downwind side than on the upwind side. This is caused by the transport of the entrained fluid towards the downwind side, and agrees closely with the entraining vortex-sheet model. The two inviscid vortex-sheet models predict completely different motions for the upwind and the downwind faces of the jet.

Experiments have shown that the deflection of the potential core is only observed for relatively large ratios λ (Rajaratnam 1976). This supports the idea that although

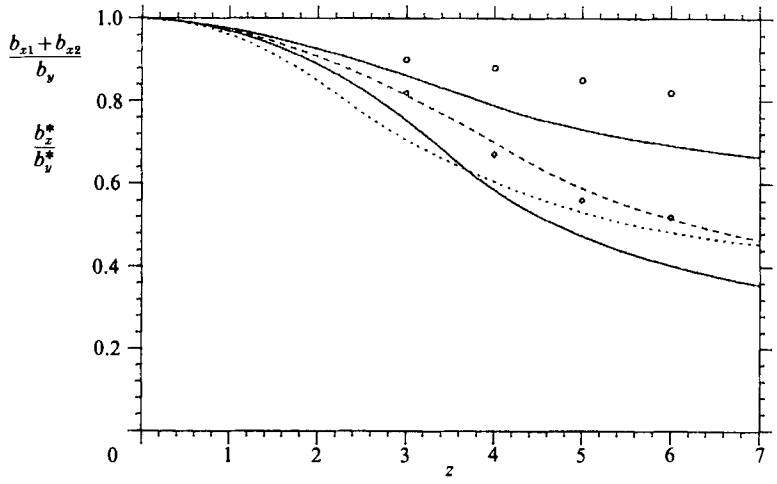

FIGURE 15. Characteristic spanwise ratios (see figure 14) for $\lambda = 0.1$. ——, entraining vortex-sheet model; – – –, 3D vortex-sheet model; · · · · ·, 2D vortex-sheet model. Top curves refer to external boundary and lower continuous curve to potential core (for $\epsilon = 0.03$). Measurements from photographs: ○, the external boundary; ◇, the potential core.

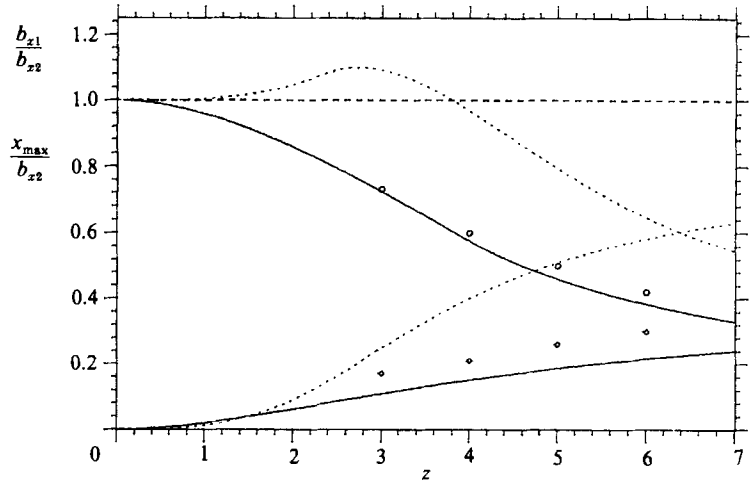

FIGURE 16. Characteristic streamwise ratios (see figure 14) for $\lambda = 0.1$. ——, entraining vortex-sheet model; – – –, 3D vortex-sheet model; · · · · ·, 2D vortex-sheet model. Top curves refer to b_{x1}/b_{x2} and lower curves to x_{max}/b_{x2} (for $\epsilon = 0.03$). Measurements from photographs: ○, the first ratio; ◇, the latter.

'pressure drag' must occur because of the formation of a wake behind the jet, it produces deformations that are negligible when compared to those induced by the addition of streamwise momentum due to entrainment.

Another test of whether a jet really acts on the external flow like a rigid cylinder is to measure the mean velocity in the (x, y)-plane along the y-axis. For solid cylinders $u_{x_{max}}/U_\infty \approx 1.4$, but according to the jet theory of §5 this value should be close to 2 for the entraining jet (see figure 17). This prediction was tested by hot-wire measurements of the total mean velocity in the (x, y)-plane ($u_p = (u_x^2 + u_y^2)^{\frac{1}{2}}$), over two planes above the exit ($z = 0.1R_0$ and $z = R_0$). Figure 17 shows that the measured

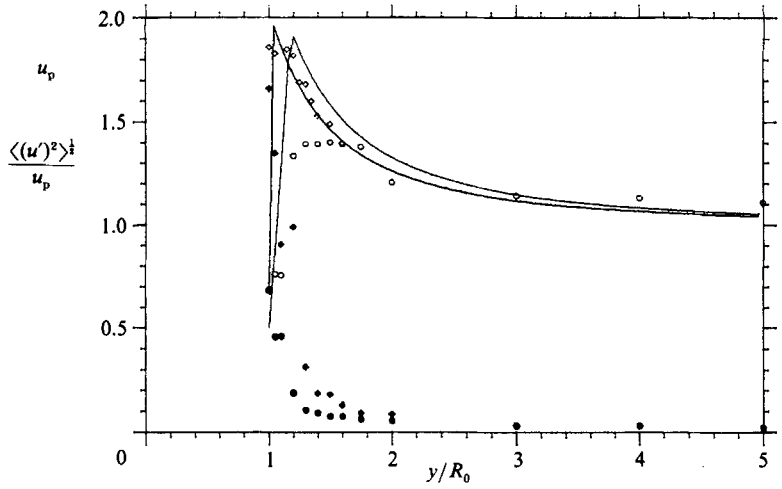

FIGURE 17. Mean velocities and turbulent intensities at $x = 0$ for the external flow about a jet issuing from a pipe ($\lambda = 0.1$). Solid lines are theoretical velocity distributions (top one for $z = 0.1R_0$ and lower one for $z = R_0$). Measured values: ○, ●, $z = 0.1R_0$; ◇, ◆, $z = R_0$. Open symbols, u_p; filled symbols, $\langle (u')^2 \rangle^{\frac{1}{2}}/u_p$.

values of u_p/U_∞ are less than the predicted values close to the pipe exit. This is because the theory assumes potential flow around the pipe, whereas in reality the flow is separated. However, within one radius above the exit the effects of the separated flow around the pipe become small; figure 17 shows how at $z = R_0$ the measured velocities of the external flow agree well with the theoretical predictions, and, in particular, with the maximum value of $u_{p_{max}}/U_\infty \approx 1.85$.

These values for u_p/U_∞ can only be obtained for the flow about a rigid circular cylinder when there is surface suction. Without suction, separation prevents this value being reached. Therefore, the drag coefficient for the jet must be smaller than that for a solid body of the same shape. Entrainment (or surface suction) reduces the width of the wake formed behind it and, consequently, reduces the wake drag. Hoerner (1965) presents a diagram showing the reduction of the wake drag with suction. However, most integral models based on pressure drag need drag coefficients of between 1.5 and 3.

Since it has been suggested by Moussa, Trischa & Eskinazi (1977) that the presence of a wall in the (x, y)-plane at the jet exit has a significant effect on the external velocity field, measurements of the velocity field around the jet were also made with a false floor, placed flush with the jet exit, that extended for three jet diameters upstream from the pipe centreline. This short length is sufficient for blocking any vertical motion near the pipe exit, and for disconnecting the flow above the jet exit from the flow around the pipe below the jet exit. But the length is short enough to avoid the building up of a boundary layer of significant thickness. Figure 18 shows that there is no significant effect of the false floor on the external flow.

The cross-sections of the jet were also photographed in the presence of this plane wall but no measurable difference in the boundaries of the shear layer was observed.

Additional experimental support for the description of the flow given by the entraining vortex-sheet model can also be found in the literature. Measurements of u_z in the near field of the flow by Kamotani & Greber (1972) and by Moussa *et al.*

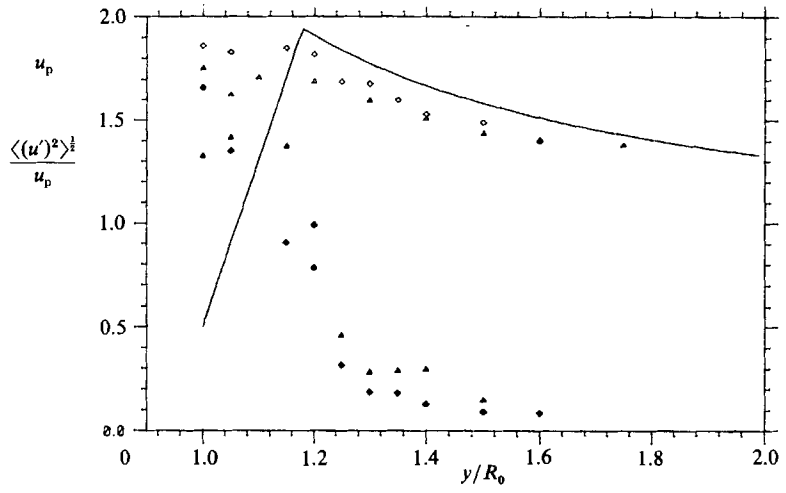

FIGURE 18. Mean velocities and turbulence intensities at $x = 0$ and $z = R_0$ for the external flow about a jet ($\lambda = 0.1$). ◇ and ◆ are measured values for a jet issuing from a pipe; △ and ▲ are for a jet issuing from a hole in a wall (no boundary layer); open symbols, u_p; filled symbols, $\langle (u')^2 \rangle^{\frac{1}{2}}/u_p$. Solid line is the theoretical velocity distribution for the first case (theory predicts small differences between the two cases).

(1977) show a rapid asymmetric change in the vertical component of the velocity along the trajectory of the jet. This supports the movement of the initially planar ring of fluid shown in figure 8.

8. Conclusions

The present analysis shows that turbulent entrainment and the transport of the transverse component of vorticity largely control the dynamics of the jet and its bounding shear layer in the near field of jets in crossflows. In particular, entrainment is the main mechanism that leads to the deflection of strong turbulent jets in the direction of the stream.

This analysis and the experiments performed show that the external flow around a strong jet is, to a first approximation, potential flow around a circular cylinder with suction, caused by the entrainment into the jet; the diffusion of vorticity into the wake is weak and therefore the jet does not act on the external flow like a solid bluff body. So, the 'pressure-drag' mechanism is negligible compared with the effects of entrainment on the deflection of the jet.

It has also been shown that Chang-Lu's unsteady two-dimensional vortex-sheet model is a basically erroneous approximation for the fully three-dimensional vortex-sheet model for the near field of these flows. The solutions obtained for this three-dimensional vortex-sheet model show that inviscid mechanisms alone are not capable of describing the dynamics of the near field. In particular, they cannot explain the deflection of the jet in the direction of the stream.

The new concepts for the vorticity dynamics that have emerged here are useful in assessing integral models for entraining jets in crossflows, and perhaps improving them. The integral models based on the entrainment mechanism only (e.g. Platten & Keffer 1968; Hoult & Weil 1972) preserve the essential features of the near field of these flows for most of the strong jets ($\lambda < 0.25$; no shift of the potential core has been observed below these ratios). For $\lambda > 0.25$ the effects of the diffusion of

vorticity into the jet's turbulent wake have to be taken into account. Some integral models that allow for this effect (by means of the 'pressure-drag' mechanism) also include the entrainment mechanism. But the combining of these mechanisms appears to be rather arbitrary.

From the engineering viewpoint, many of the existing integral models provide satisfactory descriptions for the trajectory and overall size of the jet, within specified ranges of their trajectories. However, these models have been 'tuned' for given configurations of the flow (the form of the entrainment function is arbitrarily prescribed, and the tuning constants are determined by fitting the theory to limited experimental data). They cannot be applied to different configurations of these flows without previous retuning (modifications of the arbitrary entrainment functions and new coefficients are necessary).

In addition to this, these integral models do not describe either the shape of the jet or the development of the trailing vortex pair. The circulation of these vortices ought to be calculated to improve the models of these flows, when the far field is modelled in terms of the vortex pairs. This useful approach for the far field cannot be applied to the initial bending over region.

A numerical computation of the flow that would link the 'initial conditions' at the near field, as given by the mathematical model developed in §5, to the vortex-pair solution in the far field, might be a consistent and practical way of evaluating the integral parameters and functions to be used in specific integral models for different configurations of the flow.

The analysis presented shows that numerical computations of jets in crossflows must include the effects of turbulent entrainment and the transport of the transverse component of vorticity.

It has also been shown in this paper that experiments can be and need to be devised that genuinely discriminate between different models. These tests could also be used to examine computations closely.

The authors are grateful to Dr J. W. Rottman, Mr J. H. B. Smith and the referees for helpful comments and suggestions, to Mr K. Saunders and the technicians of the CUED Aerodynamics Laboratory for their assistance, and to Conselho Nacional de Desenvolvimento Cientifico e Tecnologico-CNPq and Schlumberger Cambridge Research for financial support.

REFERENCES

ABRAMOVICH, G. N. 1963 *The Theory of Turbulent Jets*. MIT Press.

ADLER, D. & BARON, A. 1979 Prediction of a three-dimensional circular turbulent jet in cross flow. *AIAA J.* **17**, 168–174.

ANDREOPOULOS, J. & RODI, W. 1984 Experimental investigation of jets in a crossflow. *J. Fluid Mech.* **138**, 93–127.

BRAODWELL, J. E. & BREIDENTHAL, R. E. 1984 Structure and mixing of a transverse jet in incompressible flow. *J. Fluid Mech.* **148**, 405–412.

CHANG-LU, H. 1942 Aufrallung eines Zylindrischen Strahles Durch Querwind. Doctoral thesis, University of Goettingen.

DURANDO, N. A. 1971 Vortices induced in a jet by a subsonic cross flow. *AIAA J.* **9**, 325–327.

ENDO, H. 1974 A working hypothesis for predicting the path and induced velocity of a jet exhausting at a large angle into a uniform cross-flow. *Trans. Japan Soc. Aero. Space Sci.* **17**, 45–64.

FEARN, R. & WESTON, R. P. 1974 Vorticity associated with a jet in a cross flow. *AIAA J.* **12**, 1666–1671.

FOSS, J. F. 1980 Interaction region phenomena for the jet in a cross-flow problem. *Rep.* SFB 80/E/161. University of Karlsruhe.

HEAD, M. R. & BANDYOPADHYAY, P. 1981 New aspects of turbulent boundary-layer structure. *J. Fluid Mech.* **107**, 297–338.

HINZE, J. O. 1959 *Turbulence.* McGraw-Hill.

HOERNER, S. F. 1965 Fluid Dynamic Drag, pp. 3.1–3.28. S. F. Hoerner.

HOULT, D. P. & WEIL, J. C. 1972 Turbulent plume in a laminar cross flow. *Atmos. Environ.* **6**, 513–531.

HUNT, J. C. R., ABELL, C. J., PETERKA, J. A. & WOO, H. 1978 Kinematical studies of the flows around free or surface-mounted obstacles; applying topology to flow visualization. *J. Fluid Mech.* **86**, 179–200.

KAMOTANI, Y. & GREBER, I. 1972 Experiments on a turbulent jet in a cross flow. *AIAA J.* **10**, 1425–1429.

KARAGOZIAN, A. R. & GREBER, I. 1984 An analytical model for the vorticity associated with a transverse jet. *AIAA 17th Fluid Dyn. Plas. Dyn. Las. Conf.*

MAKIHATA, T. & MIYAI, Y. 1979 Trajectories of single and double jets injected into a crossflow of arbitrary velocity distribution. *Trans. ASME* I: *J. Fluids Engng* **101**, 217–223.

MARGASON, R. J. 1969 Analytical description of jet-wake cross sections for a jet normal to a subsonic free stream. *NASA Rep.* SP-218, pp. 131–139.

MASKELL, E. C. & SPENCE, D. A. 1959 A theory of the jet flap in three dimensions. *Proc. R. Soc. Lond.* A **251**, 407–425.

MILNE-THOMSON, L. M. 1960 *Theoretical Hydrodynamics*, 4th edn. Macmillan.

MOORE, D. W. 1978 The equation of motion of a vortex layer of small thickness. *Stud. Appl. Maths* **58**, 119–140.

MORTON, B. R. 1984 The generation and decay of vorticity. *Geophys. Astrophys. Fluid Dyn.* **28**, 277–308.

MOUSSA, Z. M., TRISCHKA, J. W. & ESKINAZI, S. 1977 The near field in the mixing of a round jet with a cross-stream. *J. Fluid Mech.* **80**, 49–80.

NEEDHAM, D. J., RILEY, N. & SMITH, J. H. B. 1988 A jet in crossflow. *J. Fluid Mech.* **188**, 159–184.

PAI, S. 1954 *Fluid Dynamics of Jets.* D. Van Nostrand.

PLATTEN, J. L. & KEFFER, J. F. 1968 Entrainment in deflected axisymmetric jets at various angles to the stream. *Rep.* TP 6808. University of Toronto.

RAJARATNAM, N. 1976 *Turbulent Jets – Developments in Water Sciences* No. 5. Elsevier.

ROTTMAN, J. W. & SIMPSON, J. E. 1984 The initial development of gravity currents from fixed-volume releases of heavy fluids. In *Proc. IUTAM Symp. on Atmospheric Dispersion of Heavy Gases and Small Particles, Delft*, pp. 347–359.

ROTTMAN, J. W., SIMPSON, J. E. & STANSBY, P. K. 1987 The motion of a cylinder of fluid released from rest in a cross-flow. *J. Fluid Mech.* **177**, 307–337.

SCHATZMANN, M. 1979 An integral model of plume rise. *Atmos. Environ.* **13**, 721–731.

SUCEC, J. & BOWLEY, W. W. 1976 Predictions of the trajectory of a turbulent jet injected into a crossflowing stream. *Trans. ASME* I: *J. Fluids Engng* **98**, 667–673.

SYKES, R. I., LEWELLEN, W. S. & PARKER, S. F. 1986 On the vorticity dynamics of a turbulent jet in a crossflow. *J. Fluid Mech.* **168**, 393–413.

TAYLOR, G. I. 1958 Flow induced by jets. *J. Aero. Space Sci.* **25**, 464–465.